Nanoscale and Microscale Thermophysical Engineering, 10: 109–141, 2006

ISSN: 1556-7265 print / 1556-7273 online
DOI: 10.1080/10893950600643089

A NEW CRITERION NUMBER FOR THE BOUNDARY CONDITIONS AT THE SOLID/LIQUID INTERFACE IN NANOSCALE

Yuxiu Li

Guangzhou Institute of Energy Conversion, Chinese Academy of Sciences, Nengyuan Road, Wushan, Guangzhou, China, and Graduate School of Chinese Academy of Sciences, Beijing, China

Jinliang Xu

Guangzhou Institute of Energy Conversion, Chinese Academy of Sciences, Beijing, China

A simple, but important three-atom model was proposed at the solid/liquid interface, leading to a new criterion number, λ, governing the boundary conditions (BCs) in nanoscale. The solid wall is considered as the face-centered-cubic (fcc) structure. The fluid is the liquid argon with the well-known LJ potential. Based on the concept, the two micro-systems have the same BCs if they have the same criterion number. The degree of the locking BCs is enhanced when λ equals to 0.757. Such critical criterion number results in the substantial epitaxial ordering and one, two, or even three liquid layers are locked by the solid wall, depending on the coupling energy scale ratio of the solid and liquid atoms. With deviation from the critical criterion number, the flow approaches the slip BCs and there are little ordering structures within the liquid. Always at the same criterion number, the degree of the slip is decreased or the locking is enhanced with increasing the coupling energy scale ratio of the solid and liquid atoms. The above analysis is well confirmed by the molecular dynamics (MD) simulation. The slip length is well correlated in terms of the new criterion number. The future work is suggested to extend the present theory for other microstructures of the solid wall atoms and quasi-LJ potentials.

KEY WORDS: boundary conditions, three-atom-model, criterion number, epitaxial ordering structure, slip length

INTRODUCTION

The no-slip BCs are always considered to be true in macroscale. However, when the size is down to micron or nanoscale, the no-slip BC is only one type of the various BCs [1,2]. Even though the no-slip BC has been successful in reproducing the characteristics of many types of flow, it results in singular or unrealistic behavior, such as the spreading of a liquid on a solid substrate [3,4], corner flow [5], and the extrusion of

Received 8 November 2004; accepted 9 November 2005.

The authors thank the National Natural Science Foundation of China with the contract number of 10272102 for the financial support.

Address correspondence to Jinliang Xu, Guangzhou Institute of Energy Conversion, Chinese Academy of Sciences, Nengyuan Road, Wushan, Guangzhou, 510640, China. E-mail: xujl@ms.giec.ac.cn

NOMENCLATURE

C_1	non-dimensional parameter, $C_1 = \rho_w/\rho$
C_2	non-dimensional parameter, $C_2 = \varepsilon_{wf}/\varepsilon$
C_3	non-dimensional parameter, $C_3 = \sigma_{wf}/\sigma$
F	intermolecular force between a pair of atoms
F^*	non-dimensional force, $F^* = F\sigma/\varepsilon$
F_{A-C}	force between the liquid atom and the left solid atom in the three-atom model
F_{B-C}	force between the liquid atom and the right solid atom in the three-atom model
k_B	Boltzmann's constant
L	length of a unit lattice cell
L_{AB}	length of two neighboring solid atoms based on fcc structure, $L_{AB} = L$
L_{IJ}	length between two zero force points in the three-atom-model
L_s	slip length
L_x, L_y, L_z	length of the liquid calculation domain in x,y, and z coordinates
N	liquid atom number in the calculation domain
$N_{w,top}$, $N_{w,bottom}$	top and bottom solid wall atoms
$P_1(x, y)$	spatial distribution of liquid atoms
r	distance between a pair of atoms
r^*	non-dimensional distance between a pair of atoms, scaled by σ
T_B	bulk liquid temperature
U	axial velocity
U_w	top and bottom solid wall moving velocity
x	coordinate along the line of two solid atoms, scaled by σ
x_I, x_J	locations corresponding to the zero force points in the three-atom model, scaled by σ
x_I^-, x_I^+	left and right limit of x_1, scaled by σ
x_p, x_Q	locations corresponding to the force points at which 1% of the minimal zero force points, scaled by σ
Γ	friction constant that controls the rate of heat exchange between the fluids and reservoir
$\tilde{\gamma}$	apparent shear rate
$\Delta x, \Delta y$	grid lengths in x and y directions
ε	energy scale between a pair of liquid atoms
ε_{wf}	coupling energy scale between a pair of solid and liquid atoms
η	length ratio of L_{LJ} relative to L_{AB}
$\tilde{\eta}_i$	Gaussian distributed random force with zero mean and variance $2mk_BT_B\Gamma$
λ	important non-dimensional parameter, $\lambda = C_1^{1/3}C_3$, proposed by the three-atom model
ρ	liquid atom density
ρ_w	solid atom density
σ	length scale between a pair of liquid atoms
σ_{wf}	coupling length scale between a pair of solid and liquid atoms
τ	characteristic time of Lennard-Jones atoms
ϕ	potential
ϕ_{A-C}, ϕ_{B-C}	potential between the solid atom A and the liquid atom C, and potential between the solid atom B and the liquid atom C
ϕ_{l-l}, ϕ_{l-s}	potential between a pair of solid atom and liquid atom, and potential between a pair of liquid atoms

polymer melts from a capillary tube [6,7]. An understanding of these interfacial phenomenon is essential to lubrication theories, flow and heat transfer in porous media, and deposition of a thin film on a solid substrate.

The difficulties performing a theoretical understanding of flow near solid surfaces are the limitation of the kinetic theory [1], which requires the multiple scattering of fluid atoms from individual wall molecules, which is not feasible analytically. Gas flow in microchannels have been widely studied in recent years [8], in which Knudsen number is selected as the control parameter to quantify the BCs in microchannels. Recent reviews of gas flow in microchannels can be found in Rostami et al. [9].

Liquid flow past a solid surface is quite difficult to be dealt with. This is because the liquid densities are about one thousand times of gases. The liquid molecules are always closely packed with each other and they are always in a collision state [8].

An effective tool to deal with the liquid flow past a solid interface is the MD simulations. Liem et al. [10] performed the MD simulations for simple fluid/wall interactions. The molecules at the solid wall are assumed to be the same as those of liquids, thus no-slip flow was observed. Thompson and Robbins [1] studied the Couette flow sheared by the two solid walls. They observed three types of BCs: slip, no-slip, and locking. These flow boundaries are related to the fluid structures nearest the solid walls. The no-slip or the locking BCs induce the ordering structures of the fluid layers nearest the solid walls. Such epitaxial order structure is enhanced when the solid walls have the same densities of the liquids. For unequal densities of solids and fluids, less ordering structure of the first fluid layer may produce the slip BCs. The corrugation is maximized for the equal densities of solids and fluids and the coupling energy scale is large. Under such conditions, there is sufficient momentum transfer between the solids and liquids, inducing the no-slip or even the locking BCs [1,2].

It is noted that a lot of interfacial parameters affect the flow boundaries, such as the liquid atom numbers, the apparent shear rates at the solid/liquid interfaces, the solid and liquid densities, the coupling energy scale and the length scales between solids and liquids. It is noted that the MD simulations require longer computation time and the particle numbers can be treated is also limited. To obtain a fully understanding of the flow boundary characteristics depended on the above parameters, it is necessary to perform run cases with each parameter for 10 data points for five independent parameters. This is a very large computation source and the internal relationships of the flow boundary conditions dependent on the above parameters are still difficult to identify.

In this article, a simple but efficient three-atom model was developed. We analyze the force between the liquid atom and the two neighboring solid atoms, leading to a new criterion number, λ, relating the solid/liquid densities with the coupling length scale for the solid/liquid interactions. A critical value of 0.757 for the criterion number corresponds to the no-slip or the locking BCs. Deviation from such critical criterion number causes the increased degree of slip on the boundaries. At the fixed criterion number, large coupling energy scale results in the increased degree of locking BCs, or the decreased degree of slip. The two micro-systems indeed have the same boundary characteristics if they have the same criterion number and the coupling energy scale, no matter for equal or unequal densities of solids and liquids.

The present article is organized as follows: First, we describe the proposed three-atom model, in which the last subsection describes the effect of the force interactions between the liquid atom and other solid atoms within $3\sigma_{wf}$. Then we verify the present theory by the MD simulations, including the velocity profiles and micro fluid structures near the solid walls. Next, we present the correlations of the slip length in terms of the criterion numbers, followed by a discussion of the effect of the channel height on

the BCs and the limitations of the present theory. Finally, we summarize the conclusions that were drawn in the present paper.

DESCRIPTION OF THE THREE-ATOM MODEL

In this section we present the simple, but effective, three-atom model first. The liquid atom is on the same plane of the solid wall surface interacted with the two neighboring solid molecules. At the end of this section we consider the general situation that the liquid molecule is interacted with all the solid wall molecules within $3\sigma_{wf}$ and demonstrate that the simple three-atom model is accurate enough to develop the criterion number that governs the boundary conditions at the solid wall surface.

Potential and Force Interactions among the Three Atoms

Considering the liquid argon with the non-dimensional density of $\rho\sigma^3 = 0.81$, where ρ is the liquid atom density and σ is the length scale, the length of a unit lattice cell for the liquid argon assuming the fcc structure leads to $L_{\text{argon}} = 1.7\sigma$ (note that the assumed fcc structure of the liquid atom will be melting after the initial time is passed). The Lennard-Jones potential for a pair of liquid argon atoms is written as

$$\phi_{l-l} = 4\varepsilon\left[\left(\frac{\sigma}{r}\right)^{12} - \left(\frac{\sigma}{r}\right)^{6}\right] \tag{1}$$

where ε is the energy scale and r is the distance between a pair of liquid atoms.

Now Eq. (1) is extended to consider the interaction between the solid and the liquid atoms. Figure 1 shows the Couette flow geometry, consisting of the top, the bottom walls, and the liquid argon region. The liquid region with the three lengths of L_x, L_y, and L_z is sheared by the two solid walls with the opposite flow directions at the velocity of U_w. Figure 2 illustrates the first and the second layer of the solid walls, in which the first layer is actually the solid/liquid interface. Four unit lattice cells are shown for the two layers, each with the length of L. The distance in the vertical z direction of the two solid layers is $0.5L$.

When the LJ potential, Eq. (1), is used for the interactions between the solid and the liquid atoms, the coupling energy scale ε_{wf} and the length scale σ_{wf} of the solid/liquid interactions are used instead. Defining and $C_2 = \varepsilon_{wf}/\varepsilon$ and $C_3 = \sigma_{wf}/\sigma$, the pair potential is changed to

$$\phi_{l-s} = 4C_2\varepsilon\left[C_3^{12}\left(\frac{\sigma}{r}\right)^{12} - C_3^{6}\left(\frac{\sigma}{r}\right)^{6}\right] \tag{2}$$

Using the non-dimensional length, $r^* = r/\sigma$, the non-dimensional potential is written as

$$\frac{\phi_{l-s}}{\varepsilon} = 4C_2\left(\frac{C_3^{12}}{r^{*12}} - \frac{C_3^{6}}{r^{*6}}\right) \tag{3}$$

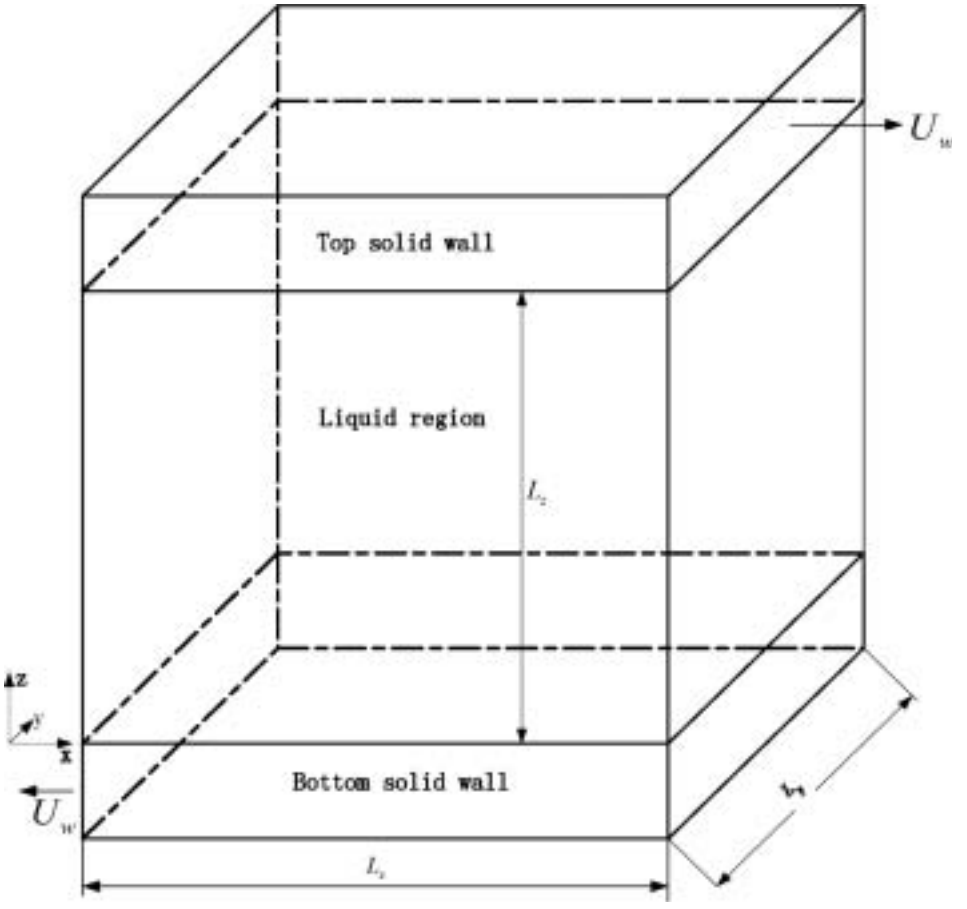

Figure 1. Couette flow geometry studied in the present article.

Using $F = -\frac{\partial \phi}{\partial r}$, the force between a pair of solid and liquid atoms in non-dimensional unit yields

$$F^* = \frac{F\sigma}{\varepsilon} = 24C_2\left(\frac{2C_3^{12}}{r^{*13}} - \frac{C_3^6}{r^{*7}}\right) \tag{4}$$

We assign the particle density of the solid atoms as ρ_w and define the density ratio relative of the solid to the liquid as $C_1 = \rho_w/\rho$. Thus, the length of a unit lattice cell for the solid wall is

$$L = 1.7\sigma C_1^{-1/3} \tag{5}$$

From Eqs. (4) and (5) it is seen that the liquid movement at the solid/liquid interface is governed by the three non-dimensional parameters, such as C_1, C_2, and C_3.

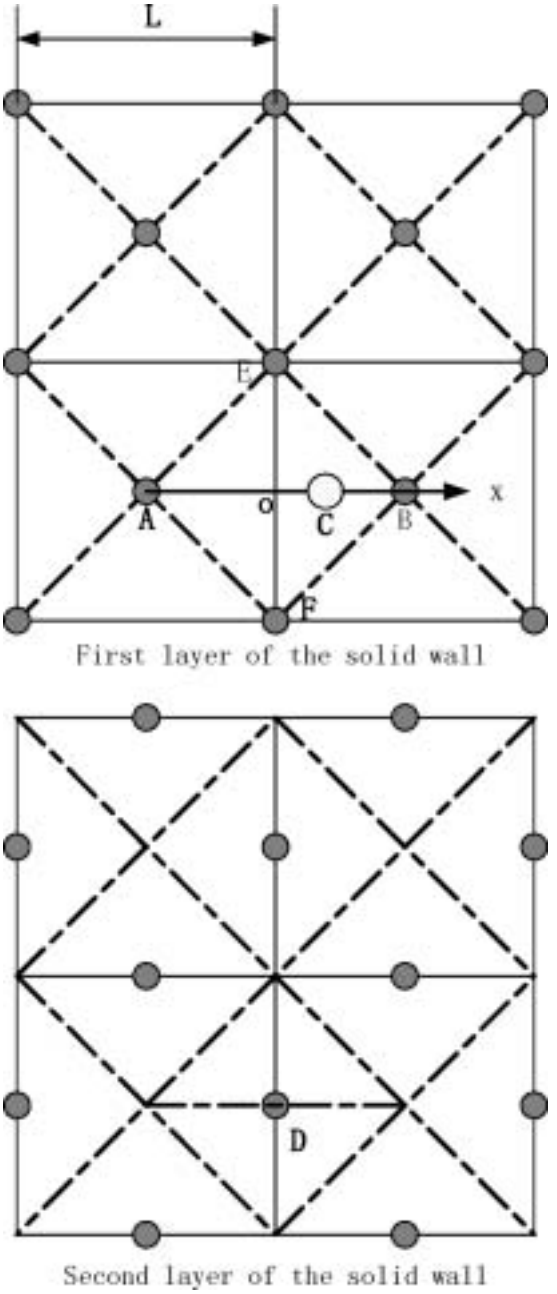

Figure 2. The first and second layer of the solid walls based on fcc structure.

We select a random unit lattice cell at the first layer of the solid wall. The four solid atoms are marked as A, F, B, and E, as shown in Figure 2. The liquid atom C is located on the line between A and B, at which a local coordinate x is attached (one-

dimensional coordinate). The center of the line AB is used as the origin of the axial. Thus, atoms A and B have the positions of $(-0.85{C_1}^{-1/3})$ and $(0.85{C_1}^{-1/3})$, scaled by σ. The molecular force interaction between the liquid atom C and the solid atoms, beyond the four neighboring particles of A, F, B, and E, are cut off due to the short distance behavior of the intermolecular forces.

When the liquid atom C is located at $x = 0$, the zero force is obtained between the liquid atom C and the four neighboring solid atoms of A, F, B, and E due to the geometry symmetry. However, if the liquid atom C is located in the regime of $0 < x < 0.85{C_1}^{-1/3}$, F_{B-C} is the largest one for the force interactions between the liquid atom C with the four neighboring solid atoms. This is because the molecular force displays the short distance behavior and the line BC has the shortest distance. The molecular force is decayed as the 13 and 7 orders exponential law with the distance. Similarly, if the liquid atom C has the positions of $-0.85{C_1}^{-1/3} < x < 0$, F_{A-C} contributes the major and domains the liquid atom flow. Based on the above analysis, when the liquid atom C is traveling on the line AB, only two forces, F_{A-C} and F_{B-C}, are necessary to consider. Later in this section we describe the effect of the liquid atom interacted with all the other solid atoms within $3\sigma_{wf}$ and demonstrate that the simple three-atom-model is accurate enough to develop the criterion number. The potentials $\phi_{A-C} + \phi_{B-C}$ and forces $F_{A-C} + F_{B-C}$ are written in the non-dimensional forms as

$$\frac{\phi_{A-C}+\phi_{B-C}}{\varepsilon} = \underbrace{4C_2\left[\frac{C_3^{12}}{(0.85C_1^{-1/3}+x)^{12}} - \frac{C_3^{6}}{(0.85C_1^{-1/3}+x)^{6}}\right]}_{\frac{\phi_{A-C}}{\varepsilon}} + \underbrace{4C_2\left[\frac{C_3^{12}}{(0.85C_1^{-1/3}-x)^{12}} - \frac{C_3^{6}}{(0.85C_1^{-1/3}-x)^{6}}\right]}_{\frac{\phi_{B-C}}{\varepsilon}} \tag{6}$$

$$\frac{(F_{A-C}+F_{B-C})\sigma}{\varepsilon} = \underbrace{24C_2\left[\frac{2C_3^{12}}{(0.85C_1^{-1/3}+x)^{13}} - \frac{C_3^{6}}{(0.85C_1^{-1/3}+x)^{7}}\right]}_{\frac{F_{A-C}\sigma}{\varepsilon}} - \underbrace{24C_2\left[\frac{2C_3^{12}}{(0.85C_1^{-1/3}-x)^{13}} - \frac{C_3^{6}}{(0.85C_1^{-1/3}-x)^{7}}\right]}_{\frac{F_{B-C}\sigma}{\varepsilon}} \tag{7}$$

Equations (6) and (7) relate the liquid atom C with the two solid atoms A and B, thus the "three-atom model" is named. The non-dimensional potential and force curves are shown in Figure 3 for $C_1 = 1.0$, $C_2 = 1.0$ with varied C_3. Another parameter, λ, is marked in Figure 3 temporarily, which equals to C_3 for $C_1 = 1.0$. However, the internal relationships among λ, C_1, and C_3 will be described later for both equal and unequal densities of solids and liquids. Seen from Figure 3a is the symmetry distribution of the potential about

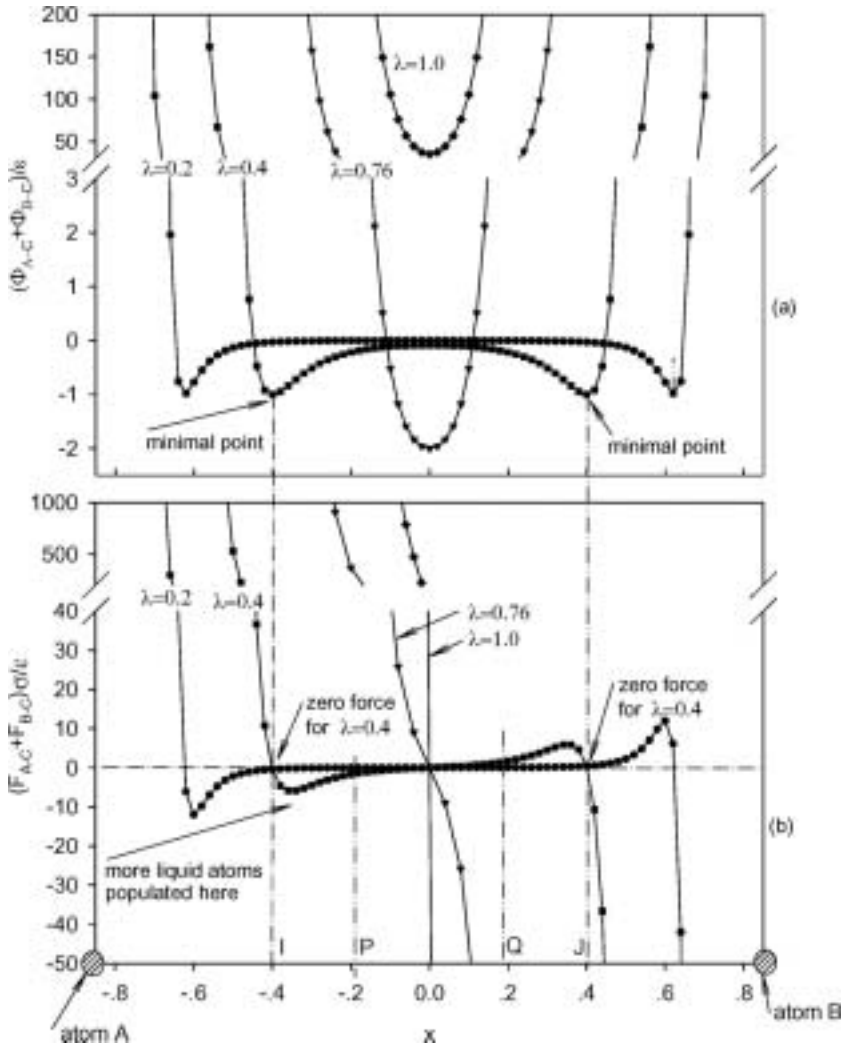

Figure 3. Potential and force between the liquid atom and the two solid atoms at the interface ($C_1 = 1.0$, $C_2 = 1.0$).

the center point of $x = 0$ (quasi-potential-well distribution). Generally, there are two minimal points of the potential, symmetrically distributed about $x = 0$. The molecular forces among the three atoms are demonstrated in Figure 3b. The two minimal points of the potential correspond to the zero forces for $\lambda = 0.4$, taking place at x_I and x_J, in which $x_I < 0$ and $x_J > 0$. For $x_I < 0$, the distance between A and I is smaller than that of between B and I; thus, F_{A-C} contributes the major part of the total force $F_{A-C} + F_{B-C}$. Solution of $F_{A-C}\sigma/\varepsilon = 0$ is accurate enough to decide the left zero force point at $x = x_I$:

$$x_I = 2^{1/6}C_3 - 0.85C_1^{-1/3} \tag{8}$$

Similarly, the right minimal point of the potential (corresponding to the right zero force point) takes place at

$$x_J = -2^{1/6}C_3 + 0.85C_1^{-1/3} \tag{9}$$

Thus, the length IJ is

$$L_{IJ} = x_J - x_I = 2(0.85C_1^{-1/3} - 2^{1/6}C_3) \tag{10}$$

Note that x_I, x_J, and L_{IJ} in Eqs. (8) to (10) are scaled by σ.

In Figure 3b, the positive force represents the direction toward the right (atom B), while the negative force indicates the direction toward the left (atom A). Three regions of the forces are identified and they are related to the BCs, which are described as follows.

1. The high repulsive force region ($-0.85{C_1}^{-1/3} < x < x_I$ and $x_J < x < 0.85C_1^{-1/3}$). Liquid atoms can not be populated in this region due to the high repulsive force with very steep gradient versus the x coordinate.
2. The liquid atom metastable region ($x_I < x < x_P$ and $x_Q < x < x_J$). Because these two regions shared the interfaces with the high repulsive force region at $x = x_I$ and $x = x_J$, the liquid atoms are in oscillating and metastable state along the line IP or QJ. Imagining a liquid atom is located between I and P, the attractive force from the solid atom A extracts the liquid atom toward the solid atom A. However, once the liquid atom crosses the position of $x = x_I$, the high repulsive force will push the liquid atom back to the region of $x_I < x < x_P$. Such process repeats and the oscillating state is maintained. Moreover, we imagine that a cluster of liquid atoms on the line AB, the attractive force in the region of IP draw more liquid atoms populated in this region, especially at the local area of $x = {x_I}^+$. The interface at $x = {x_I}^-$ forms a barrier that prevents the liquid atoms penetrating the location of $x = x_I$. In Figure 3b $x = x_P$ is selected at which the force is only 1% of the minimal force. The force at $x = x_P$ is very close to be zero.
3. The liquid atom free population region ($x_P < x < x_Q$). Because the force in this region is very close to zero, liquid atoms can be freely populated. Imagining the solid wall is moving at a speed of U_w suddenly, the liquid atom may not respond to such movement of the solid wall due to the zero force induced by the solid wall. Thus, slip BC occurs if the liquid atom stays in this region.

The Criterion Number λ and its Effect on the Boundary Conditions for λ < 0.757

Based on the above description, liquid atoms cannot be populated in the region of AI and BJ, but can be populated in the region of IJ, much more densely populated in the attractive force region of IP and QJ. Defining the length ratio of the length IJ

relative to the whole lattice length of AB as η:

$$\eta = \frac{L_{IJ}}{L_{AB}} = \frac{2(0.85C_1^{-1/3} - 2^{1/6}C_3)}{1.7C_1^{-1/3}} = 1 - 1.32C_1^{1/3}C_3 \tag{11}$$

η is directly related to the BCs. The limit case is $\eta = 0$, indicating that the two zero force points shown in Figure 3b shrinks to one at $x = 0$. Beyond the center point of the two solid atoms at $x = 0$, very large force pushes the liquid atom back to $x = 0$. Once the solid wall is traveling at a speed, the liquid atoms will follow the movement of the solid wall, inducing the no-slip or even the locking BCs. Inversely, a large η yields a longer area for the free populated liquid atoms relative to the whole lattice length. Imagining the solid wall is moving, the liquid atoms in the "free populated region" may not respond to such movement of the solid wall, resulting in the enhanced slip of the liquid atoms on the solid/liquid interface.

Here we introduce a criterion number, $\lambda = C_1{}^{1/3}C_3$. Note that η and λ have the linear relationship with a constant slope of -1.32 ($\eta + 1.32\lambda = 1$). Physically, λ is equal to 0.757 times of the two lengths of the "high repulsive force region" over the whole length of a unit lattice length. Referring to Figure 3, λ can be expressed as

$$\lambda = 0.757 \times \frac{L_{AI} + L_{BJ}}{L_{AB}} \tag{12}$$

where L_{AI} and L_{BJ} are the left and right length of the high repulsive force region, referring to Figure 3. The larger λ is, the smaller η is, corresponding to the shorter free populated region of the liquid atoms and the degree of slip is decreased, providing $\eta > 0$. The dependent of λ and the length of L_{IJ} is shown in Figure 3b for $\lambda = 0.2, 0.4, 0.76$ and 1.0.

In Eq. (11), $\lambda = C_1^{1/3}C_3 = 0.757$ causes $\eta = 0$, corresponding to the no-slip or the locking BCs. Incorporating the following analysis, $\lambda = 0.757$ is a critical value at which the slip BCs is minimized. In addition to these, λ is a very important parameter controlling the BCs.

The Effect of the Solid Atom D on the Boundary Conditions for $\lambda > 0.757$

As shown in Figure 3b, if λ is further increased larger than 0.757, such as $\lambda = 1.0$, the potential and force curves show the similar shape as those at $\lambda = 0.757$. However, the $F_{A-C} + F_{B-C}$ force curve has a very steep gradient near $x = 0$. From appearance it seems that the no-slip or locking BCs is enhanced with increasing λ for $\lambda > 0.757$. However, our MD simulation results do not support this conclusion. In fact, the degree of no-slip or locking BCs is decreased with further increasing λ if $\lambda > 0.757$. The reason is coming from the force interaction between the liquid atom C and the solid atom D of the second layer (see Figure 2). In terms of the fcc structure of the solid walls, the solid atom D is just below the center point of the line AB by in the vertical plane (xz plane, see Figure 4a). The force direction between the atom D and C is along the line DC in the vertical plane. Seen from Figure 4 is that for $\lambda \leq 0.757$, the potential ϕ_{D-C} and F_{D-C} are quite smaller than those between the liquid atom C and the solid atoms A and B in the horizontal plane (xy plane) along the whole

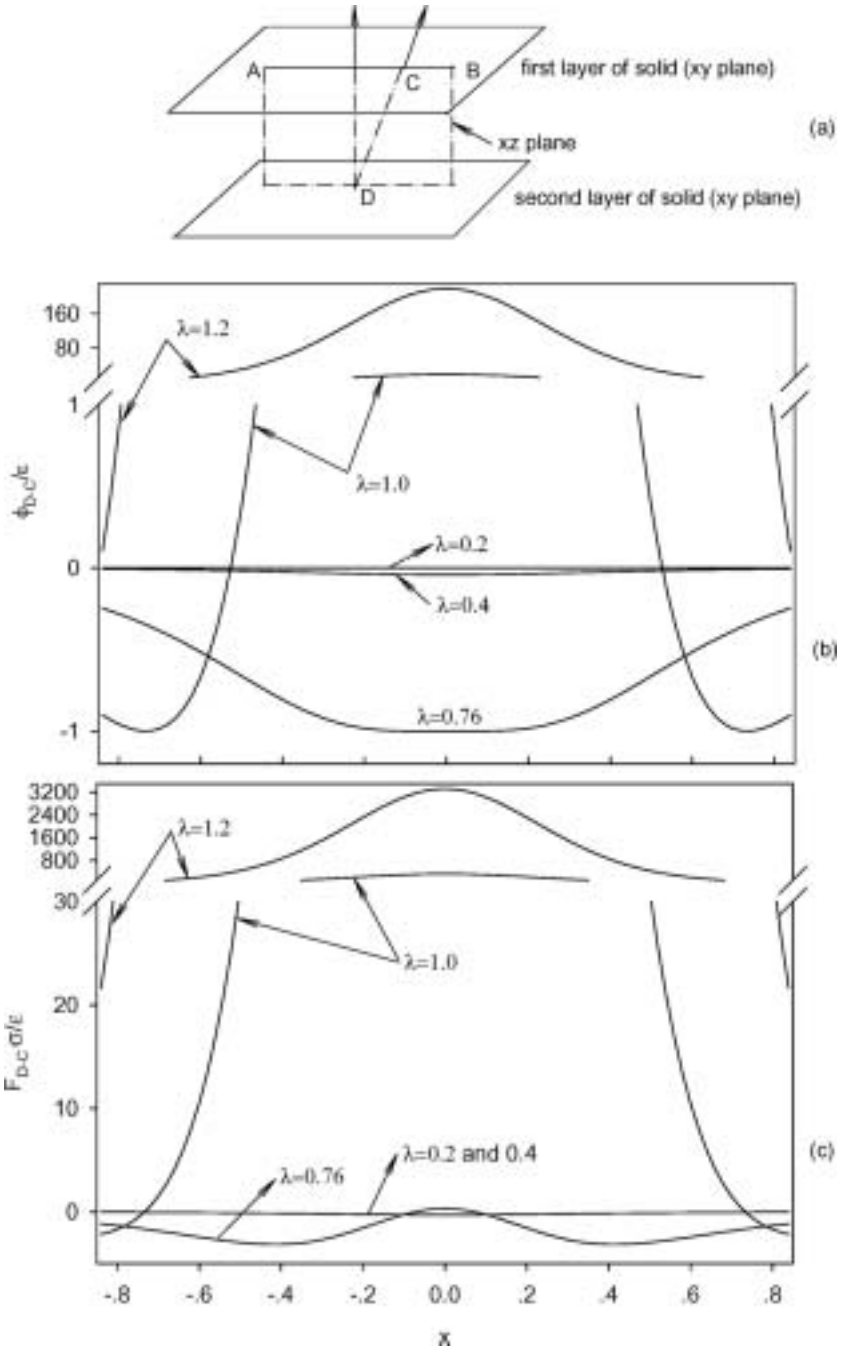

Figure 4. Potential and force between the solid atom D and the liquid atom C for different λ ($C_1 = 1.0, C_2 = 1.0$).

length of AB; thus, a very weak effect of the solid atom D on the BCs is obtained. However, when $\lambda > 0.757$, such as $\lambda = 1.0$ and $\lambda = 1.2$, the potential ϕ_{D-C} and F_{D-C} are quite large compared with those between the liquid atom C and the solid atoms A and B (see Figure 4). Note that F_{D-C} is in the vertical plane (xz plane) and the negative value indicates the attractive force. The high repulsive force of F_{D-C} quickly pushes the liquid atom C away from the solid wall to the liquid region. Thus, the liquid atom C cannot be populated on the solid wall surface stably, leading to the increased degree of slip.

Thus, incorporating the analysis in the previous subsection, the no-slip or locking BCs is enhanced when $\lambda = 0.757$. Deviation from such critical value causes the increased degree of slip.

Effect of C_2 on the Boundary Conditions

Among the three parameters C_1, C_2, and C_3, there is a criterion number $\lambda = C_1^{1/3} C_3$. At a fixed C_2, the two micro-systems would have the same BCs providing they have the same λ, which can be used as a scale law.

Seen from Figure 3 and 5 is that even though the liquid particles can be populated in the region between the two zero force points, large attractive forces are induced by increasing the energy scale ratio, C_2. This effect can cause more liquid particles located in the liquid atom metastable region, forming higher peak distributions of liquid particles in this region. Thus, the degree of slip is decreased, or the degree of locking is enhanced. C_2 is another parameter affecting the BCs, independent of λ.

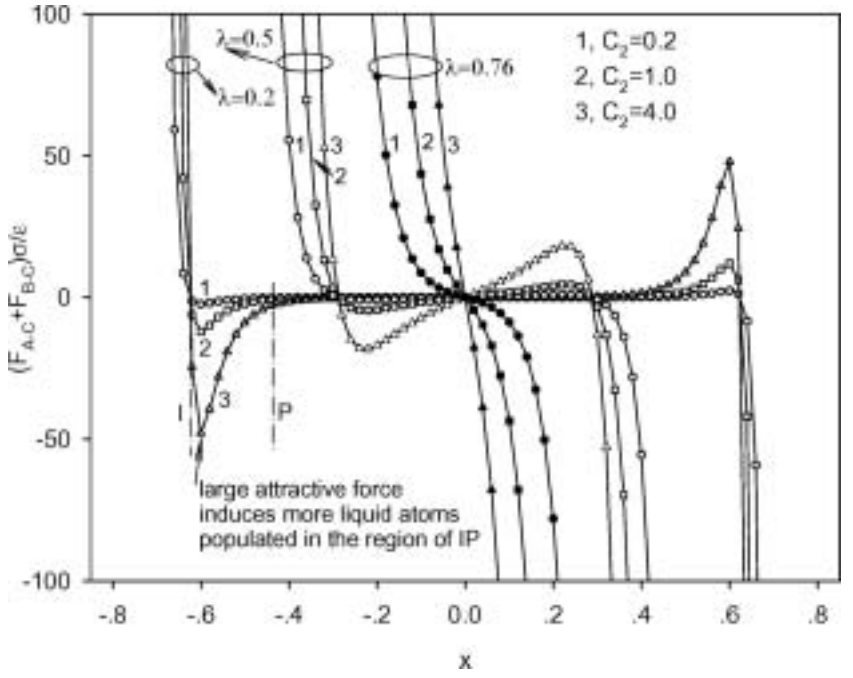

Figure 5. Combined effect of λ and C_2 on the force between the liquid atom and the two solid atoms ($C_1 = 1.0$).

Figure 5 shows three curve groups, with $\lambda = 0.2$, 0.5, and 0.76, respectively. There are three curves in each group, each corresponds to $C_2 = 0.2$, 1.0, and 4.0. For a certain group of λ, increasing C_2 leads to higher attractive force, inducing more liquid particles populated in the region of IP, causing the degree of slip to decrease.

Effect of the Force Interactions between the Liquid Atom and Other Solid Atoms within $3\sigma_{wf}$

We have so far described a simple three-atom-model that leads to a new criterion number. Now we analyze the potential and force interactions between the liquid atom and the solid atoms within $3\sigma_{wf}$; note that the cutoff distance between a pair of atoms is $2.5\sigma_{wf}$. The objective of this subsection is to demonstrate that the three-atom model is accurate enough to develop the criterion number that governs the BCs. Figure 6 shows a more general arrangement of the solid atoms in terms of the fcc structure, in which five layers of the solid atoms are included layer by layer. Each solid atom has a certain position of (x, y, z). Again a random cell is selected, consisting of the four solid atoms marked as A, F, B, and E. The liquid atom C on the top surface of the solid atoms, which can be anywhere in the area of AFBE, is marked by the small sphere. The coordinate is set as shown in Figure 6. If the liquid atom C is in the area of AFBE, the potential for the liquid atom over all the solid atoms selected can be written as

$$\phi/\varepsilon = \frac{\phi_{A-C} + \phi_{B-C}}{\varepsilon} + \frac{\phi_{E-C} + \phi_{F-C}}{\varepsilon} + \frac{\sum \phi_{i-C}}{\varepsilon} \tag{13}$$

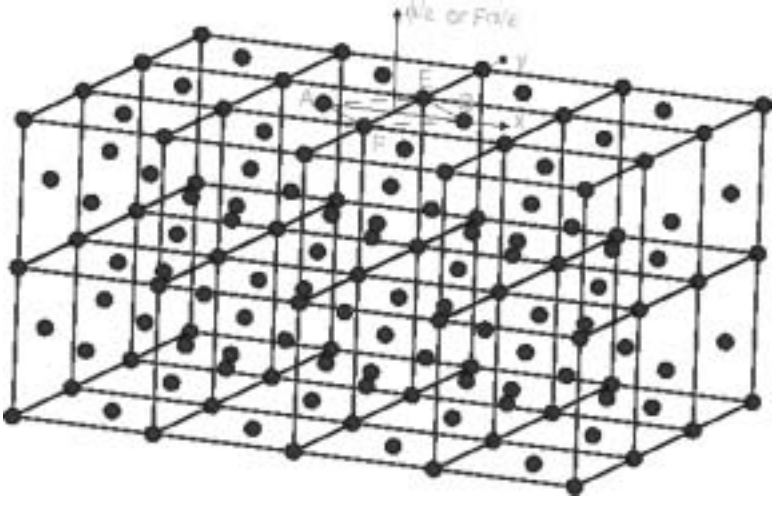

Figure 6. Solid atom arrangements for the polyatomic interactions between the liquid atom and the solid atoms within $3\sigma_{wf}$.

The intermolecular force in the x direction between the liquid atom and all the solid atoms selected is written as

$$F\sigma/\varepsilon = \frac{(F_{A-C,x} + F_{B-C,x})\sigma}{\varepsilon} + \frac{(F_{E-C,x} + F_{F-C,x})\sigma}{\varepsilon} + \frac{\sum F_{i-C,x}\sigma}{\varepsilon} \tag{14}$$

In Eqs. (13) and (14), i is any solid atom other than A, F, B, and E. The subscript x represents the x component.

The computed results are shown in Figures 7–8, for $\lambda = 0.2$, 0.4, and 0.76 with the fixed $C_2 = 1.0$. In Figures 7 and 8, the left column indicates the three-dimensional distributions of the polyatomic integrations, while the right column represents the comparison between the polyatomic integrations and the three-atom model with the liquid atom fixed in the line AB. The right columns (two-dimensional distribution) are the vertical cross sections that cross the line AB of the three-dimensional distributions. It is shown that the polyatomic interactions matched the predictions by the three-atom model well for both of the potential and the axial forces when the liquid atom is traveling along the line AB. This is because the distance between the liquid solid atom C and the solid atom A or B always has the smallest value if the liquid atom is in line AB. The strong short distance potential and force interaction behavior leads to the domain contributions of the solid atom A and B. Thus, considering the intermolecular interactions among the three atoms of A, B, and C is accurate enough for the BCs. One exception is that the potentials computed by the polyatomic integrations is higher than those by the three-atom model when λ equals to 0.76 (see Figure 7c). This is why we need to consider the solid atom D in the second layer (see Figure 2) to analyze the BCs.

VERIFICATIONS BY THE MOLECULAR DYNAMICS

Description of the MD Simulation Model

The previous studies of the MD simulation for the BCs by Thompson and Robbins [1,2] stated that the no-slip BC ($L_s = 0$) occurs at the equal densities of solids and liquids. The epitaxial ordering structure for the fluid layers nearest the solid wall is induced at large $C_2 = \varepsilon_{wf}/\varepsilon$. Higher solid densities decreased the effective corrugation of the solid wall and reduced the fluid layer ordering structure. Such effect increased the degree of slip at small $C_2 = \varepsilon_{wf}/\varepsilon$. However, the present theory shows that even at the unequal densities of the solids and liquids, the no-slip or locking BCs can still happen if the criterion number λ is close to 0.757. Using λ as the similarity scale law, the two micro-systems would have the same BCs if they have the same criterion number. In this section we demonstrate how the important information given by the present theory is verified by the MD simulations.

The MD simulations were performed referring to Figure 1. The three-dimensional coordinates are set as x, y and z, as shown in Figure 1. There are $N = 864$ liquid atoms for the liquid calculation domain. Because a unit lattice cell has four particles for the initial fcc assumption, six unit lattice cells are distributed in each of the three directions ($4 \times 6^3 = 864$), corresponding to the cubic arrangement of $L_x = L_y = L_z = 10.22\sigma$ for the liquid calculation domain. The top and bottom solid atoms involved in the calculation are dependent on the density ratio of C_1 and the length scale ratio of C_3. For instance, there are $N_{w,top} = N_{w,bottom} = 294$ solid particles selected for each

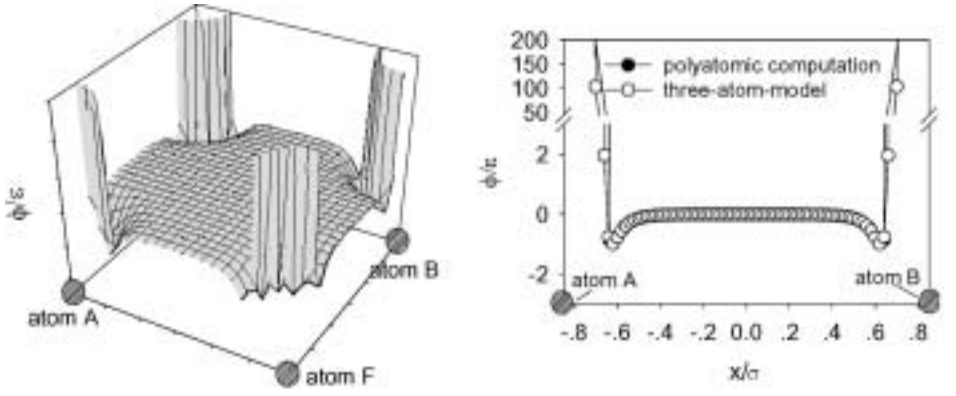

(a) $\lambda = 0.2, C_2 = 1.0$

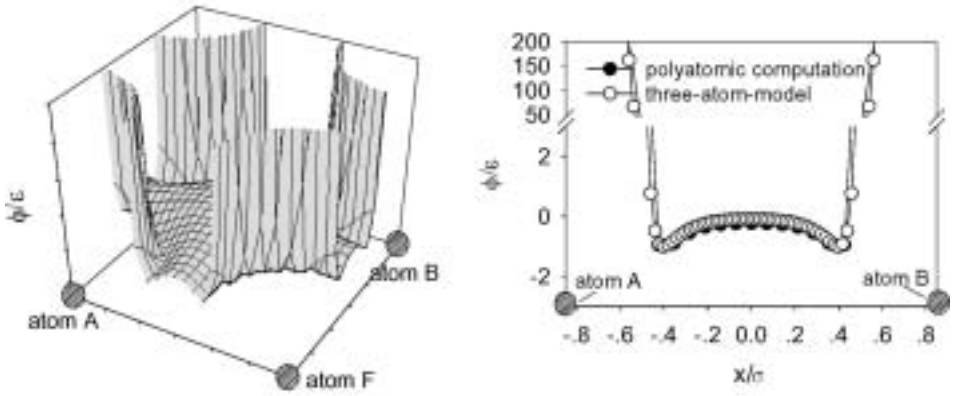

(b) $\lambda = 0.4, C_2 = 1.0$

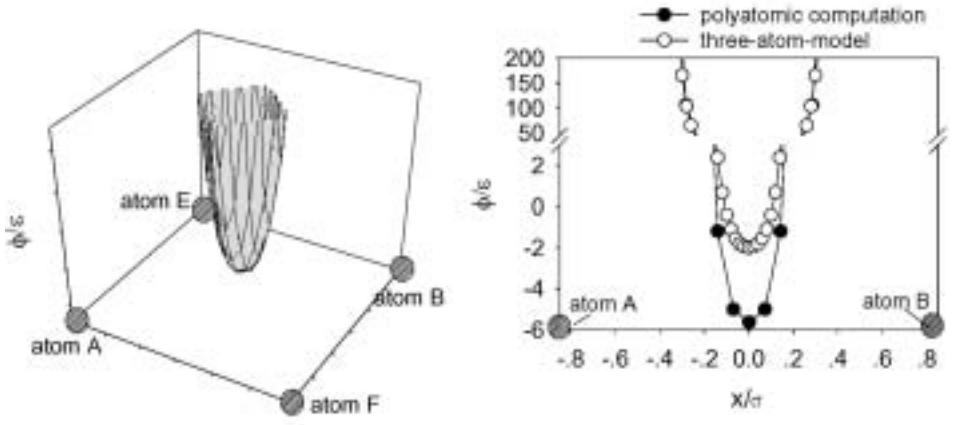

(c) $\lambda = 0.76, C_2 = 1.0$

Figure 7. Polyatomic potential interactions between liquid atom and the solid atoms within $3\sigma_{wf}$.

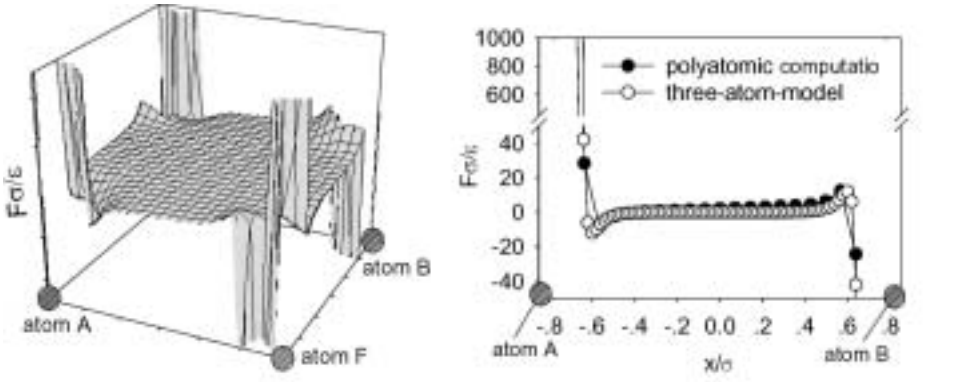

(a) $\lambda = 0.2, C_2 = 1.0$

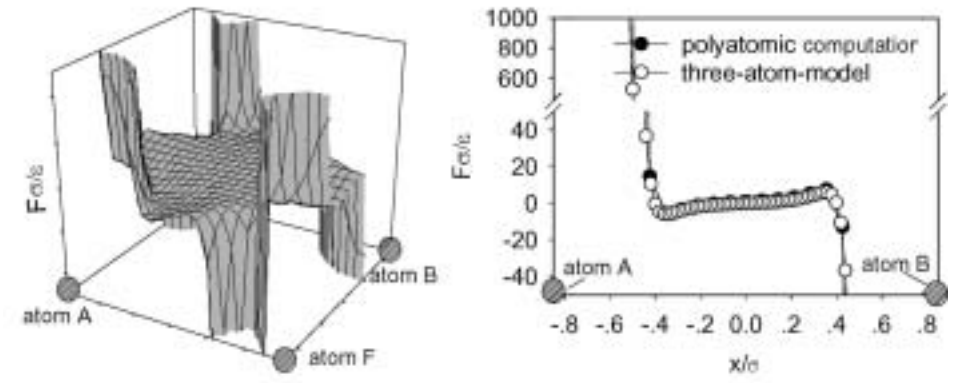

(b) $\lambda = 0.4, C_2 = 1.0$

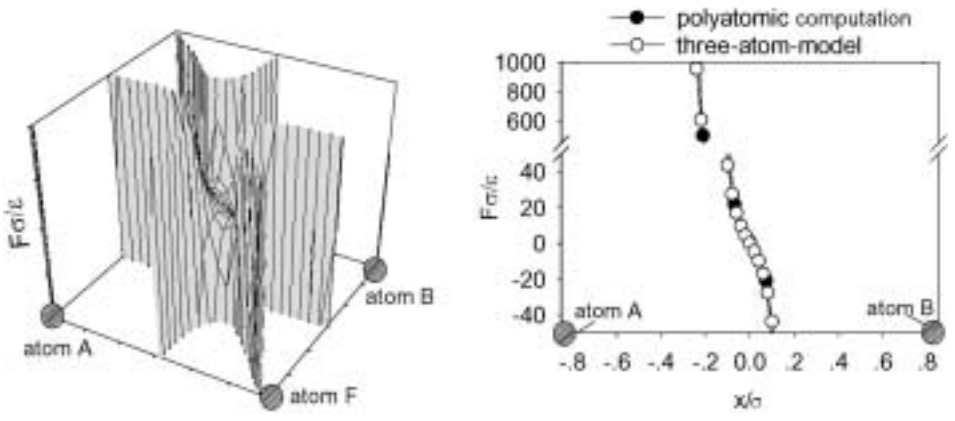

(c) $\lambda = 0.76, C_2 = 1.0$

Figure 8. Polyatomic force interactions between liquid atom and the solid atoms within $3\sigma_{wf}$.

wall for $C_1 = 1.0$ and $C_3 = 0.8$. However, there are $N_{w,top} = N_{w,bottom} = 800$ solid atoms taking part in the calculation for $C_1 = 4.63$ and $C_3 = 1.0$. The run case of $C_1 = 4.63$ is the highest solid density one studied in the present article. Such geometry arrangement satisfies that the distance between the liquid atoms on the solid/liquid interface and any solid atoms can be truncated at $r_{cut} = 2.5\sigma_{wf} = 2.5C_3\sigma$, while the cutoff distance among the liquid atoms is set as 2.5σ.

We consider the intermolecular forces not only among the liquid atoms, but also between the liquid atoms and the solid walls. Outside of the calculation domain, the periodic boundary conditions are applied in x and y coordinates. For the startup of the MD simulations, initial conditions are set for the liquid particle positions, velocities, and higher order derivatives. The initial positions of the liquids are set as fcc structure, which will melt after the MD simulations are performed. A random initial velocities of the liquid particles are assumed, but scaled by the liquid temperatures, $T_B = 1.1k_B/\varepsilon$. The initial particle accelerations are decided based on the positions of $r_1(0)$ by computing the forces on each atom and applying Newton's second law. The initial higher order of derivatives are assumed to be zero, but will be updated following the MD simulations.

The MD simulations performed the force integration for each liquid atom in the calculation domain and applied Newton's second law. The fifth-order gear finite-difference algorithm was used. The argon characteristic time is written as $\tau = (m\sigma^2/\varepsilon)^{0.5}$. The time step is chosen in the range of $\Delta t = 0.005$–0.0005τ, depending on the BCs. For no-slip or locking BCs, $\Delta t = 0.005\tau$ is small enough. However, with increasing the degree of slip, a shorter time step is needed.

It is noted that the shear flow inside the Couette flow geometry is not only governed by the four parameters of C_1, C_2, C_3, L_z, but also on the fluid pressures and temperatures. Because we consider the liquid instead of gas, the fluid pressure has almost no effect on the shear flow. This behavior is similar to the fact that the physical properties such as specific heat, thermal conductivity, etc., are mainly dependent on the temperatures, very weakly dependent on the pressures. During the MD simulation, the solid atoms are fixed as fcc structure, but the whole body of the two solid walls are moving in opposite directions to form the Couette flow. This assumption indicates the zero temperatures of the solid walls. The liquid temperatures are fixed as $T_B = 1.1k_B/\varepsilon$. Shearing the fluid molecules inside the two solid walls leads to the viscous dissipation that warms up the system. A common technique for removing heat entails the *ad hoc* rescaling of the instantaneous atomic velocities $\mathbf{v}$. However, before the steady-state flow field is reached, velocity rescaling may bias the flow field. In order to overcome this problem, we maintain constant liquid temperature by introducing damping and Langevin noise terms to the equations in v_y [1,2]. The resulting equation of motion for the y direction is written for the ith molecule of mass m as

$$m\ddot{y}_i = \sum_{j\neq i,j=1}^{N} F_{ij,y} + \sum_{j_w=1}^{N_w} F_{ij_w,y} - m\Gamma\dot{y}_i + \tilde{\eta}_i \tag{15}$$

where the first term of the right-hand side represents the force in the y direction integrated over all the liquid molecules, the second term represents the force in the y direction over all the solid molecules considered, Γ is a friction constant that controls the rate of heat exchange with the reservoir, and η_i is a Gaussian distributed random

force with zero mean and variance $2mk_BT_B\Gamma$. The third and fourth terms of the right-hand side are the damping and noise terms respectively. The MD simulations show that the effect of the damping and noise terms on the steady-state flow field is decreased with decreasing the apparent shear rate ($\gamma = 2U_w < /L_z < 1\tau^{-1}$). This is easy to understand because the smaller the shear rate is, the less viscous heat is generated. Since the y component is perpendicular to the shear plane, using the damping and noise terms in the y component can successfully remove the heat produced by the viscous heat dissipation. A similar procedure is successfully applied in Thompson and Robbins [1] and Thompson and Troian [2]. Our previous paper [11] shows that the computed flow field is well consistent with that given by Thompson and Troian [2] for a special run case.

Generally, after the initial 150τ is elapsed, the system has evolved into the steady state. The macroscopic parameters such as velocity profiles are stable. The liquid calculation domain is divided into 24 bins in the z direction. Each bin has the plane area of $L_x \times L_y$ that equals to that of the calculation domain, but with the thickness of $\Delta z = 0.425\sigma$. The numerical integrations for the parameter averaging, including the velocities and the non-dimensional densities $\rho\sigma^3$, at each center of the selected bin, were averaged from 150τ to 300τ.

We calculate the spatial distribution $P_1(x,y)$ of liquid atoms for the first, second, and third layers nearest the solid walls. For each liquid layer, a set of lattice cells in the xy plane were divided. Each lattice cell is exactly corresponding to those of the solid walls in the xy plane with a gap in the z direction. The four corners and the center of the lattice cell correspond to the positions of the relative solid particles located in the xy plane. There are 24×24 grids divided in each lattice cell, with $\Delta x = \Delta y = L/24$, where L is the length of a unit lattice cell. We count the liquid particles that fall into the local area of $[(x,x + \Delta x),(y,y + \Delta y)]$ in each grid, with the thickness of Δz. Such statistical counting was averaged over 150τ and the area of $\Delta x \times \Delta y$ after the initial 150τ passed.

Velocity Profiles Depended on λ and C_2

For the Couuete flow, the slip BCs correspond to the linear velocity profiles across the two solid walls, but the velocity differences occur at the solid/liquid interface. The exact no-slip BCs have the velocity profiles, exactly the same as the classical solutions in macroscale. The locking BCs have curve velocity profiles showing the same velocities as the solid wall at the interface but varied velocity gradients nearest the wall. For the Couette flow with the opposite flow directions of the two solid walls, the center point at $z = L_z/2$ also has the zero mean velocities. We plot a linear line that passes through ($z = L_z/2, U = 0$) with the slope as the same as that of the curve fit of the computed velocity profile at the center point. The straight line is extended to $U/U_w = 1$. The slip length as L_S is defined from this point to the solid wall. The no-slip, locking, and slip BCs correspond to $L_S = 0$, $L_S < 0$, and $L_S > 0$, respectively. The slip length characterizes the degree of slip or locking at the interface.

Figure 9 shows the velocity profiles dependent on λ and C_2. Seen from Figure 9a is that when $\lambda = 0.8 \rightarrow 0.757$, the flow approaches the no-slip or the locking BCs. With increasing C_2 from 0.2 to 4.0, the flow switches from the quasi-no-slip BCs (velocity profiles dotted by "•" for $C_2 = 0.2$ and "■" for $C_2 = 0.6$) to the locking BCs (curves dotted by "▲" for $C_2 = 1.8$ and "▼" for $C_2 = 4.0$). For the locking BCs, the velocity

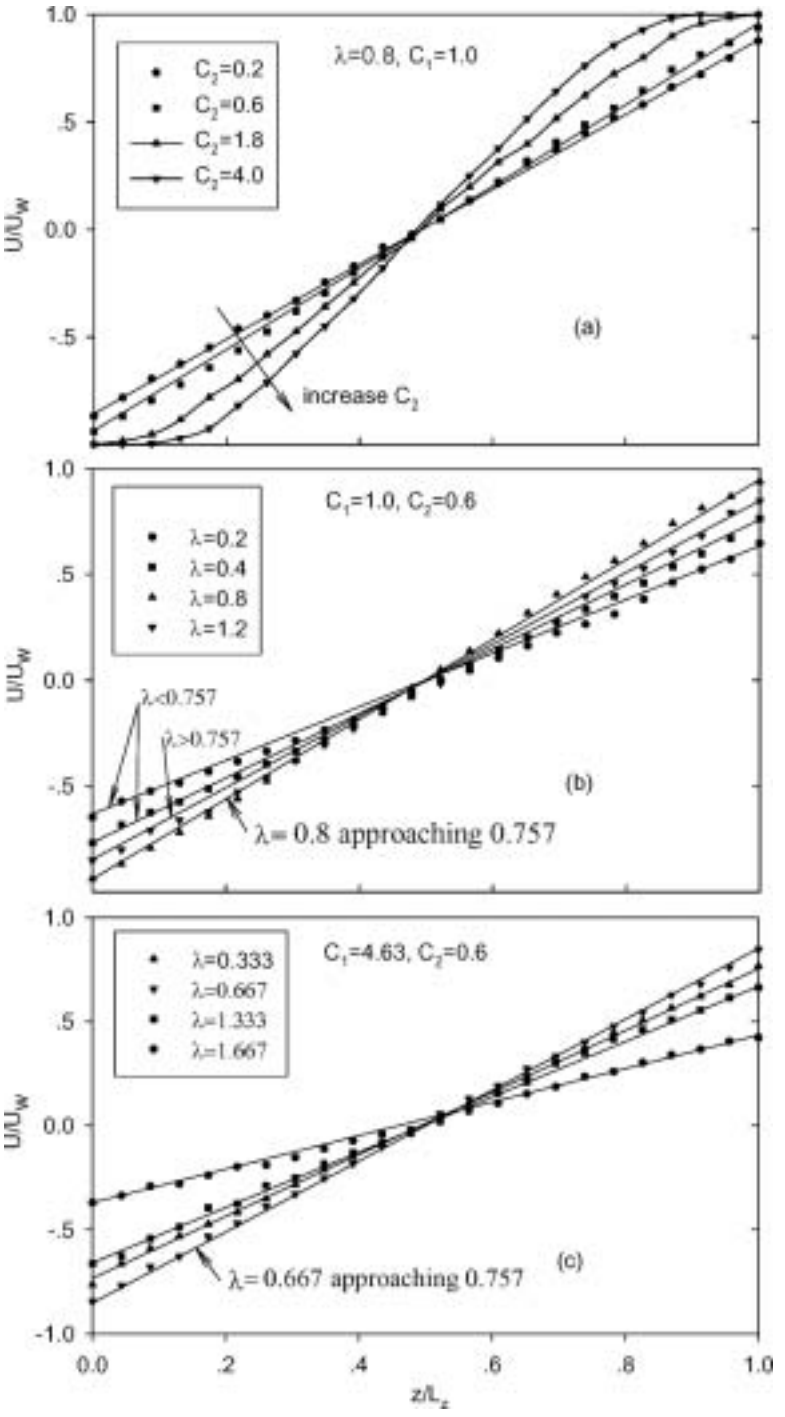

Figure 9. Effect of λ and C_2 on the velocity profiles for the Couette flow.

profiles are not the straight lines. The velocity gradients near the solid wall are very gentle for several liquid layers, corresponding to the epitaxial order structure in these layers, which will be described later. Figures 9b and 9c illustrate the velocity profiles for the equal and unequal densities of the solids and liquids, $C_1 = 1.0$ and $C_1 = 4.63$, both with $C_2 = 0.6$. The two figures show that when λ approaches 0.757, the flow approaches the quasi-no-slip BCs. Smaller or larger λ than the critical value of 0.757 leads to the increased degree of slip.

Figure 9 tells us that indeed the velocity profiles are dependent on λ and C_2. The no-slip BCs can also be approached even at the high density ratios of solids and liquids. The MD simulation results support the three-atom model and the criterion number theory.

Effect of λ on the Micro Liquid Structure Nearest the Solid Wall at the Fixed C_2

Figure 10 shows the velocity profiles and the first layer of fluid structures nearest the solid wall, for the two micro Couette flow geometries with the same size of liquid computation domain, λ and C_2. However, the two micro-systems have different C_1 (density ratio) and C_3 (length scale ratio), but these two parameters are coordinated to keep the same $\lambda = C_1^{1/3} C_3$. It is seen that indeed the two Couette flows remain the same velocity profiles and very close first layer liquid structures, at the same $\lambda = 0.4$ and $C_2 = 0.6$. Even though the two Couette flow geometries have the different lengths of a unit lattice cell, 1.7σ for Figure 10b and 1.27σ for Figure 10c, due to the different solid atom densities, the peak values of $P_1(x,y)$ are nearly the same, indicating the same liquid structures and the corresponding BCs. The center and the four corners of the unit lattice cell shown are directly related to the positions of the crystallized solid atoms located in the xy plane. We relate $P_1(x,y)$ shown in Figure 10b to the three-atom model shown in Figure 2. One of the solid atom, such as the solid atom A, shown in Figure 2, is located at the center of the unit lattice cell in Figure 10b, and the other solid atom, such as the atom B, is positioned at the center of the unit lattice cell for a neighboring lattice cell, shown in Figure 10b. Note that the $P_1(x,y)$ for a unit lattice cell shown in Figure 10 is a two-dimensional distribution (xy plane), while the three-atom model is actually a one-dimensional model. Figures 10b and 10c are the run cases for the moderate slip BCs and little ordering of the fluid structure occurs, but the peak of the $P_1(x,y)$ can still be identified, which is located in the attractive force region close to the zero force point corresponding to Figure 3 for the force curve at $\lambda = 0.4$, as proposed by the three-atom model.

Another comparison between the two micro Couette flows for the quasi-no-slip BCs is shown in Figure 11. It is noted that indeed when $\lambda = 0.8 \rightarrow 0.757$, the no-slip BC is approached, no matter for equal or unequal densities of the solids and liquids. The four peaks of the $P_1(x,y)$ distributions are taking place at the centers between the two solid atoms, forming the "extended" fcc structure of the solid walls, which is called the "epitaxial ordering structure."

Further increasing λ larger than 0.757, such as 1.2, as shown in Figure 12, the flow transitions to the slip BCs, even though the order liquid structure of the first layer can still be identified. The $P_1(x,y)$ peak value of 0.0071 is 2.4 times smaller than that for the case at which $\lambda = 0.8$ shown in Figure 11b. $I_s = 0.60\sigma$ is larger than $L_s = 0.19\sigma$ shown in Figure 11b, indicating the degree of slip is increased when λ excesses the

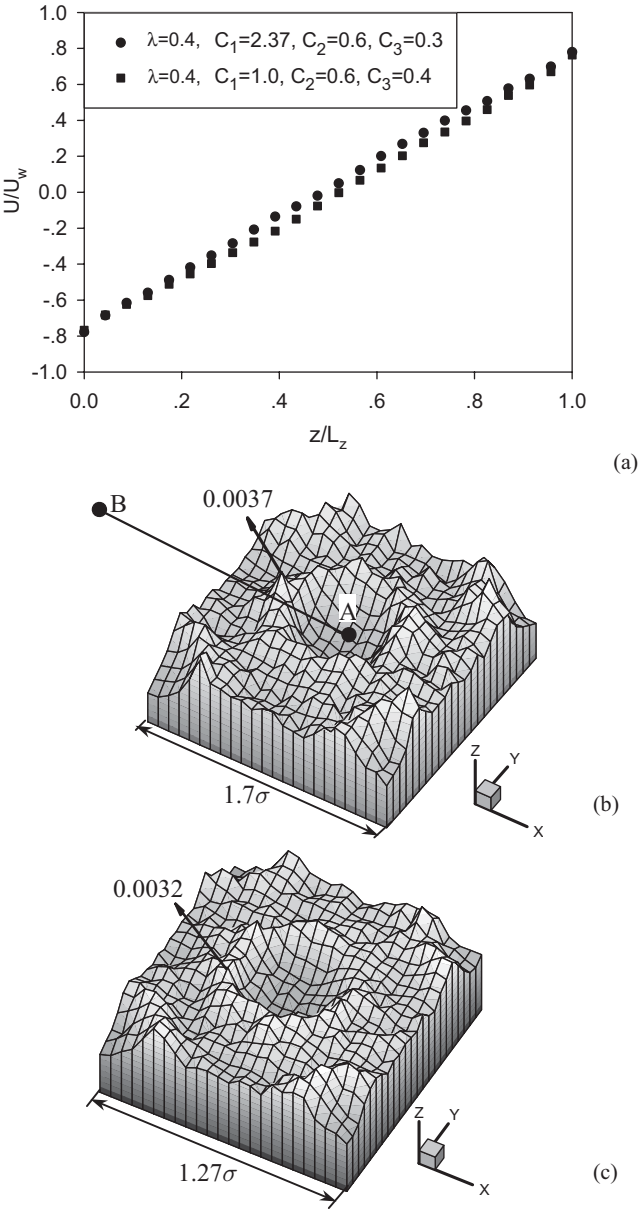

Figure 10. Comparison of the velocity profiles and $P(x, y)$ at $\lambda = 0.4$, $C_2 = 0.6$ for slip BCs. (a) Velocity profiles, (b) $P(x,y)$ for $C_1 = 1.0$, $C_3 = 0.4$, $L_S = 1.49\sigma$, (c) $P(x,y)$ for $C_1 = 2.37$, $C_3 = 0.3$, $L_S = 1.63\sigma$.

critical value of 0.757. The reason is coming from the potential and force interactions between the liquid atoms and the solid atom D of the second solid layer, explained in Figure 4.

Comparing Figures 10 to 12, it is seen that the liquid layer ordering structure is indeed enhanced when λ approaches 0.757.

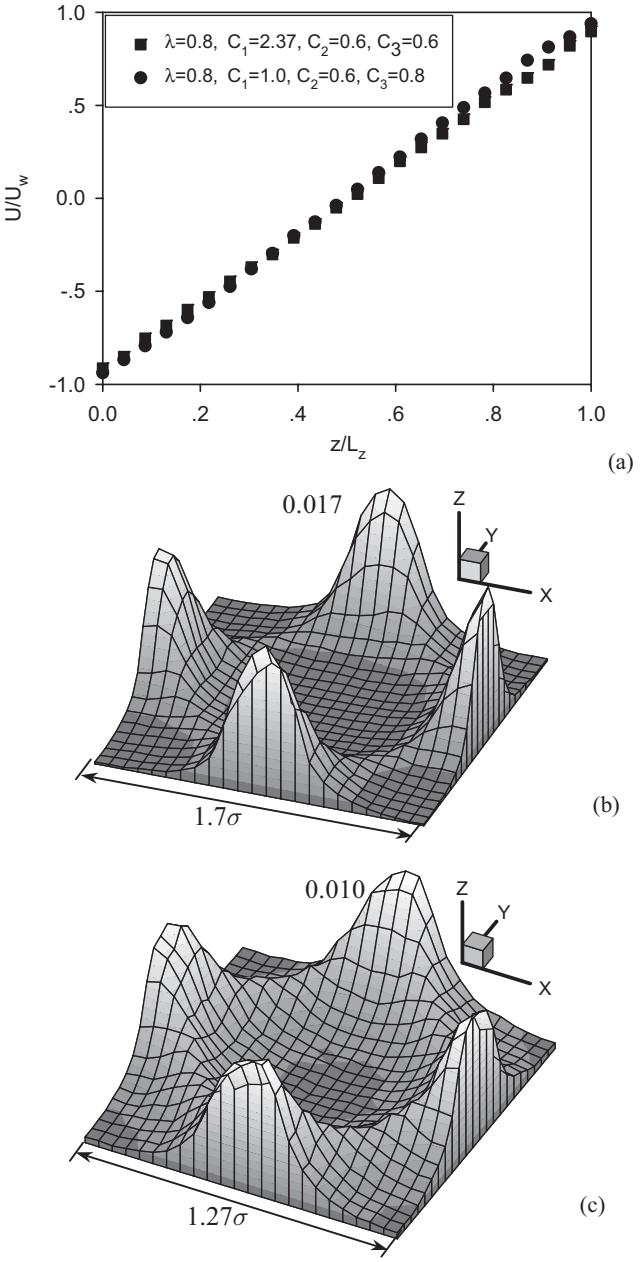

Figure 11. Comparison of $P(x,y)$ at $\lambda = 0.8$, $C_2 = 0.6$ for quasi-no-slip BCs. (a) Velocity profiles, (b) $P(x,y)$ for $C_1 = 1.0$, $C_3 = 0.8$, $L_S = 0.19\sigma$, (c) $P(x,y)$ for $C_1 = 2.37$, $C_3 = 0.6$, $L_S = 0.24\sigma$.

Effect of C_2 on the Micro Fluid Structure Nearest the Solid Wall

As analyzed above, at a given λ, increasing C_2 induces higher possibilities that liquid particles populated in the local attractive force region between the two solid

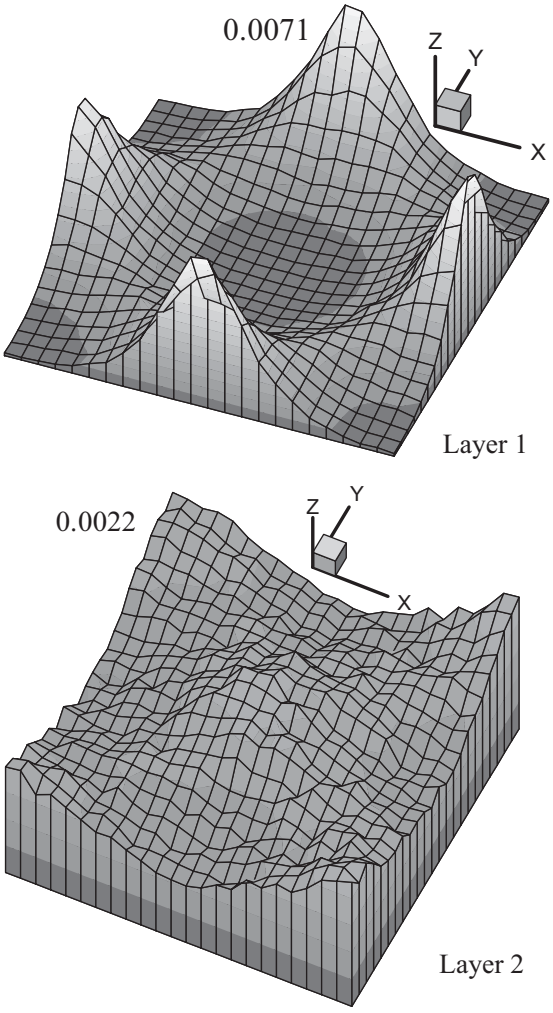

Figure 12. $P(x,y)$ for the first and second layer of the fluids nearest the solid wall at $\lambda = 1.2$, $C_1 = 1.0$, $C_2 = 0.6$, $C_3 = 1.2$, $L_S = 0.60\sigma$.

atoms, as shown in Figure 5. Such an effect induces the decreased degree of slip, or the increased degree of locking, depending on λ. The effect of C_2 on the liquid layer structure can be identified by comparing Figure 13 and Figure 10b, in which $\lambda = 0.4$ for both of the figures. But the higher C_2 in Figure 13 results in ordering distributions of $P_1(x,y)$, while little ordering structure of the first fluid layer nearest the solid wall was seen for smaller C_2 in Figure 10b.

The locking BCs are much enhanced when the criterion number $\lambda = 0.757$ and a larger C_2. Such conclusion is verified by Figure 14, in which $\lambda = 0.8$, $C_2 = 4.0$. The substantial ordering structure for the $P_1(x,y)$ can be extended successively from the first liquid layer, which is nearest the solid wall, to the third liquid layer. The liquid particles are locally located at the center of the two solid atoms for the first layer. Checking the peak values of the $P_1(x,y)$ distributions shows that the degree of the

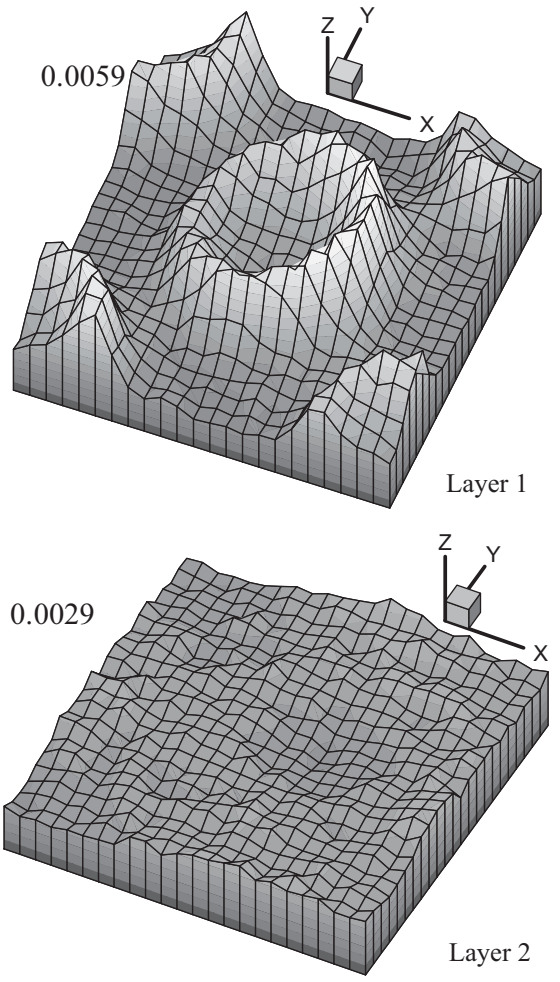

Figure 13. Effect of C_2 on the $P(x,y)$ for the first and the second layer of the fluids nearest the solid wall (λ = 0.4, C_1 = 1.0, C_2 = 1.8, C_3 = 0.4, $L_S = 0.64\sigma$, compared with Figure 10b).

ordering structure was gradually decreased for the second and third liquid layers. Up to the fourth fluid layer, a uniform $P_1(x,y)$ distribution begins to be established. The fluid structures of first, second, and third layers form the fcc structure, extending the fcc structure of the crystallized solid wall.

CORRELATIONS OF THE SLIP LENGTH IN TERMS OF λ AND C_2

Slip length characterizes the degree of slip occurring at the solid/liquid interface. Figure 15 illustrates L_S versus C_2 for equal (C_1 = 1.0) and unequal densities (C_1 = 4.63) of solids and liquids. L_S is smallest when the criterion number λ is approaching 0.747 (curve dotted by "■" for equal density of solid and fluid, Figure 15a). For unequal densities of solids and fluids (C_1 = 4.63 as shown in Figure 15b), L_s is smallest for λ equals to 0.667 and 0.8333. Smaller or larger criterion numbers than the critical

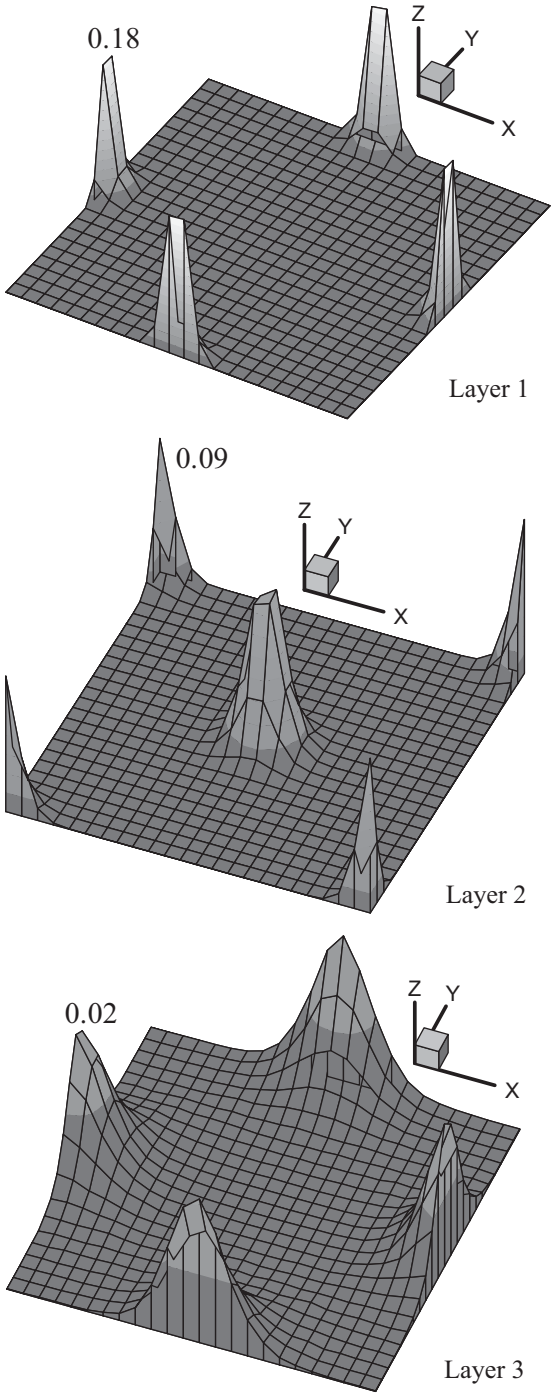

Figure 14. Effect of C_2 on the $P(x,y)$ for the first, second, and the third layer of the fluids nearest the solid wall ($\lambda = 0.8$, $C_1 = 1.0$, $C_2 = 4.0$, $C_3 = 0.8$, $L_S = -1.76\sigma$, compared with Figure 11b).

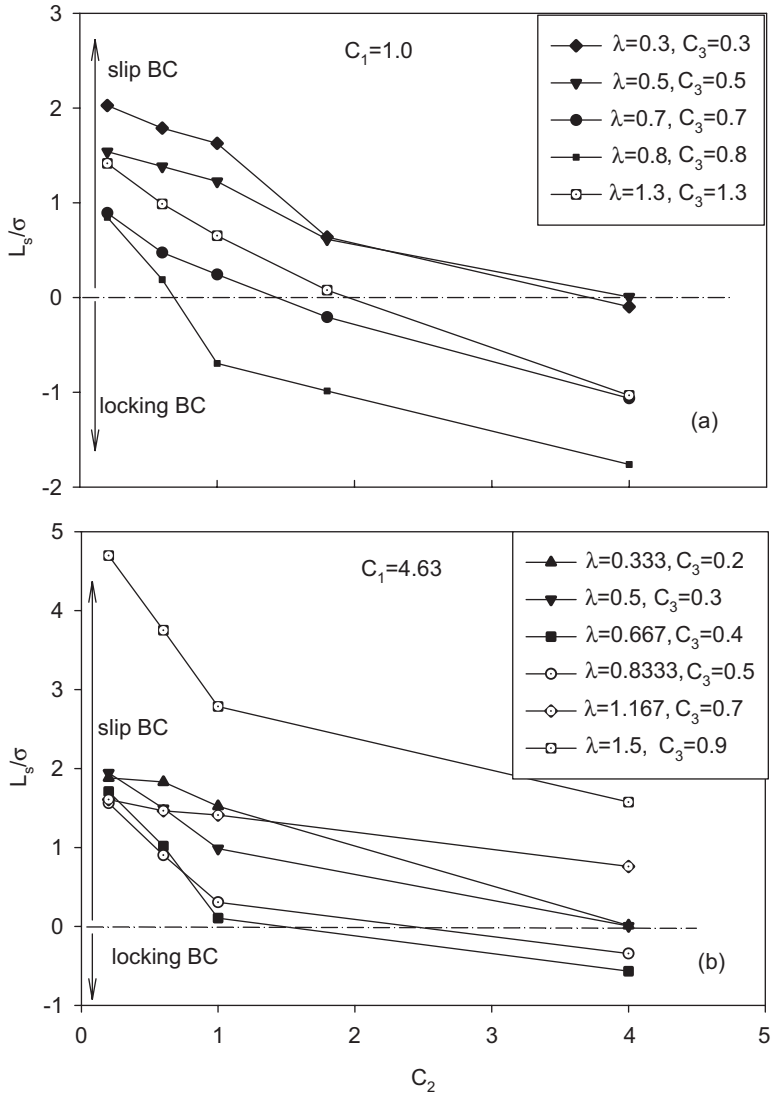

Figure 15. Effect of C_2 on the slip length.

value increase the degree of slip if C_2 is fixed. When λ is close to 0.757, the flow can switch from the slight slip BCs (positive L_s) to the no-slip BCs ($L_S = 0$) with continuous increasing C_2. Further increasing C_2 induces the locking BCs (negative L_S). In Figure 15 it can be seen that even when the solid wall atoms are more densely populated than the liquids, the no-slip and locking BCs can still be obtained if λ is close to the critical value of 0.757.

Figure 16 demonstrates the relationships between L_s and C_3. It is quite clear that the minimal L_s takes place at the critical criterion number λ for unequal densities of solids and fluids ($C_1 = 4.63, C_3 = 0.454$ corresponding to $\lambda = 0.757$). For equal

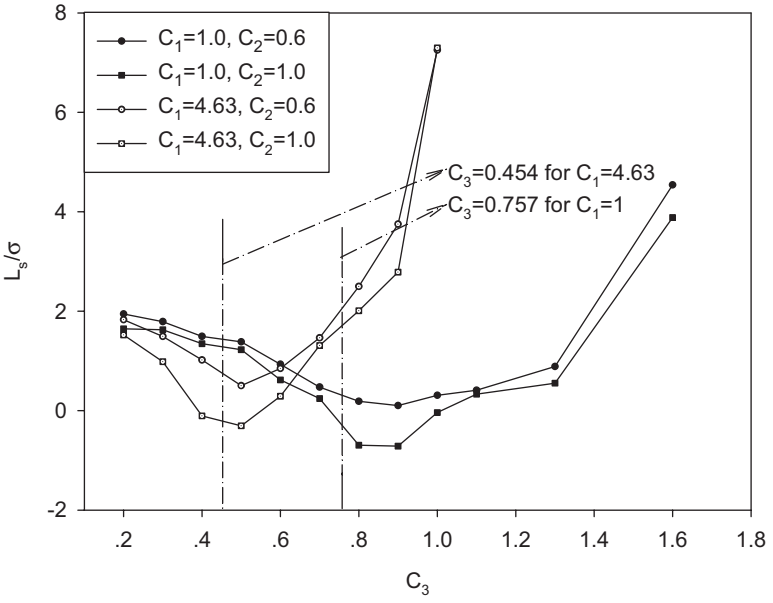

Figure 16. Effect of C_3 on the slip length at two different C_1.

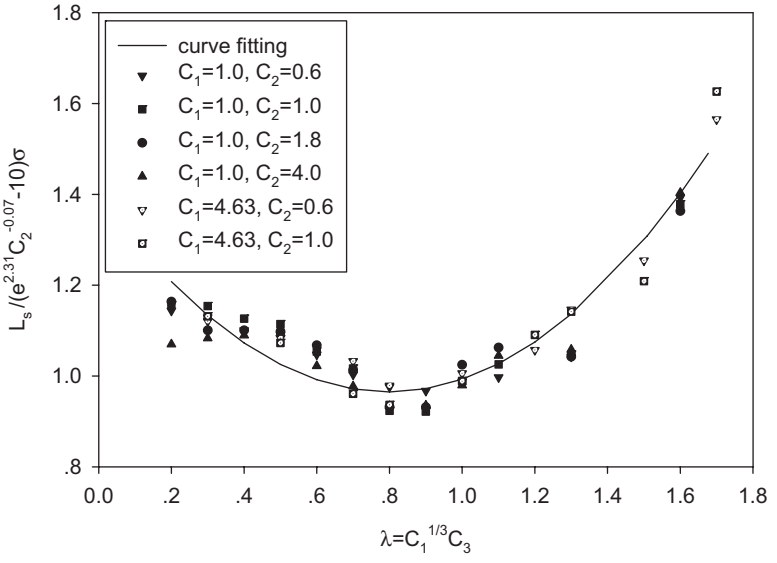

Figure 17. Correlation of the slip length based on the criterion number, $\lambda = C_1^{1/3} C_3$.

densities of solids and fluids, the minimal L_s has a little deviation from the line of $\lambda = 0.757$ ($C_1 = 1.0, C_3 = 0.757$).

Correlation of L_s is given in Figure 17 explicitly depended on λ and C_2. Such correlation process involves two steps. The first step is to develop the

relationship of L_s and C_2 at different λ for the equal density system. Such process results in a correlation of

$$L_s^0 = e^{2.31} C_2^{-0.07} - 10 \tag{16}$$

The second step is to correlate $L_s/L^0{}_s$ versus the criterion number, λ, for both equal and unequal densities of the solids and fluids in Figure 17. It is not surprising to note that all the data points fall into nearly a single curve with the minimal L_s taking place at the λ of 0.798, which is close to the critical value of $\lambda = 0.757$, as proposed by the three-atom model. The minimal L_s taking place at two different C_3 in Figure 16 can be incorporated into a single minimal point using the criterion number as the scale law, as shown in Figure 17. Finally, we give the parabola curve correlation corresponding to Figure 17 as

$$\frac{L_s}{L_s^0} = 0.975 + 0.165 \times (\lambda - 0.92) + 0.680 \times (\lambda - 0.92)^2 \tag{17}$$

The above correlations use the 66 data points, covering the ranges of λ from 0.2 to 1.67, C_1 from 1.0 to 4.33, C_2 from 0.6 to 4.0, and C_3 from 0.2 to 1.4. The maximum error between the slip lengths computed by MD simulations and Eq. (14) is 8.37%.

SIZE EFFECT ON THE BOUNDARY CONDITIONS

In this section we analyze the BCs with varied channel height. Again, the MD simulations were performed and verified by the three-atom model. Three channel heights were modeled with $L_z = 11.05\sigma$, 31.45σ, and 51.85σ, respectively, in which $L_z = 51.85\sigma$ is almost the maximum height that our computer can analyze. The velocity profiles and Pr distributions were presented in Figures 18–20 for the slip, no-slip, and locking BCs, respectively. In each of these figures, the left column gives the velocity profiles and the right column gives the Pr distributions. We performed these computations at the fixed apparent shear rate of 0.05, which is defined as $\gamma = 2U_w/L_z$. We define the slip velocity U_{sp} as the velocity difference between the solid wall and the liquid molecules at the interface. For the locking BCs, the velocity profiles are not linear. U_{sp} is defined as the velocity difference between the solid wall and the extended linear fit of the velocity profile in the center region across the two channel walls, as shown in Figure 20. U_{sp} is positive, zero, and negative for the slip, no-slip, and locking BCs, respectively. For the slip BC run as shown in Figure 18, U_{sp} is 0.13, 0.11, and 0.12 for the three channel heights of 11.05σ, 31.45σ, and 31.45σ, respectively. Incorporating the almost similar Pr distributions for the three channel heights, we conclude that the BCs are almost independent of the channel height. When $\lambda = 0.7 \rightarrow 0.757$ (see Figure 19), the no-slip BCs are approached for all three channel heights. U_{sp} is almost zero and the epitaxial order structure begins to be established. The strong locking behavior occurs for all the channel heights with $\lambda = 0.76 \approx 0.757$ and large C_2 of 4.0, as shown in Figure 20. Again, the negative U_{sp} is nearly the same and very similar Pr distributions occur. It is seen that indeed the BCs mainly rely on the criterion number and C_2, independent of the channel height, reflecting the physical mechanism of the intermolecular potential and force interactions near the solid/liquid interface. The independent effect of the channel height on the BCs is consistent with the conclusion given in Thompson and Robbins [1].

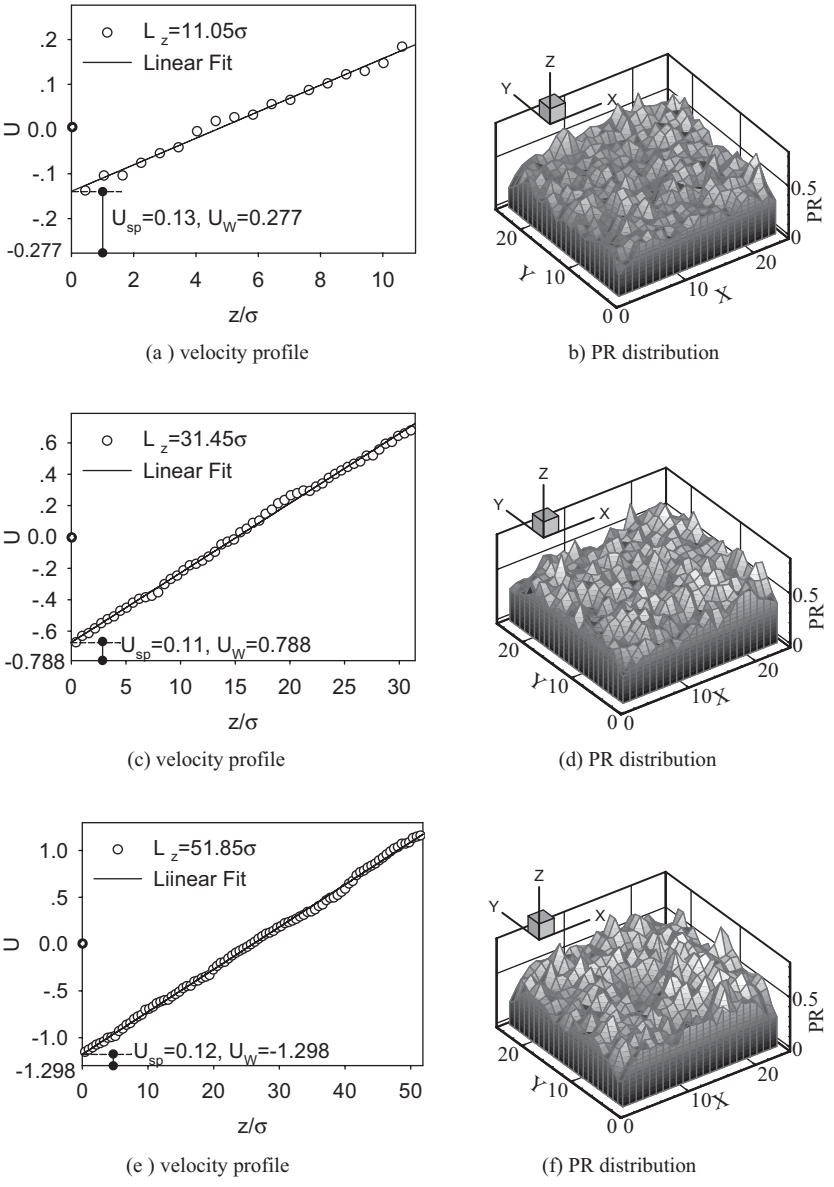

Figure 18. Velocity profile and Pr distributions for three channel heights, $C_1 = 1.0$, $C_2 = 0.2$, $C_3 = 0.3$, $\gamma = 0.05$.

LIMITATION OF THE PRESENT THREE-ATOM MODEL

The present three-atom model is limited by the fcc structure of the solid wall atoms (<111>crystal plane) and the well-known LJ potential, which are widely applied in MD simulations. The liquid is specified as the liquid argon. It is noted that the fcc structure is crystal structure in nature [12]. Solids consist of atoms that are bound together by chemical bonds. These atoms sometimes are arranged in an ordered and periodic array called a crystal. A crystal is formed by repeating a unit cell in all directions. The most

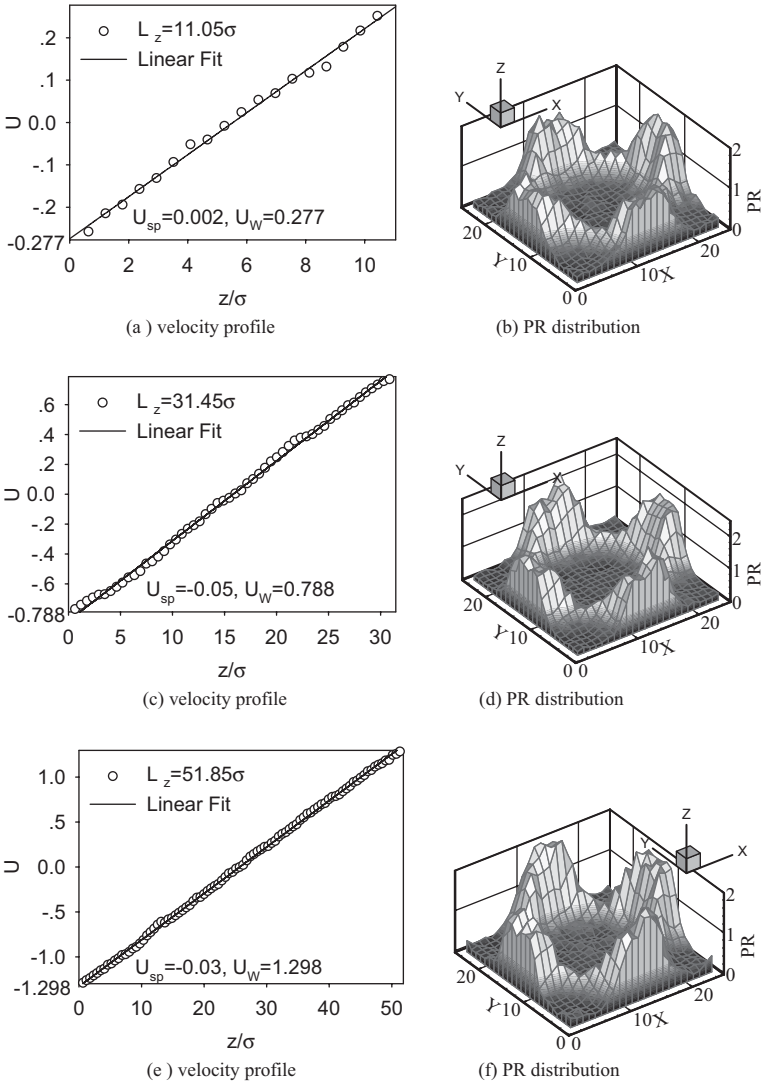

Figure 19. Velocity profile and Pr distributions for three channel heights, $C_1 = 1.0, C_2 = 1.0, C_3 = 0.7, \gamma = 0.05$.

important crystal structures are the simple cubic and the hexagonal closed packaged structures. Derivations of the simple cubic structure include the body-centered cubic (bcc), the face-centered cubic (fcc), and the diamond structure. The detailed description of the natural microstructures of solids can be found in Rupaport [13].

The second issue involved in the three-atom model is the intermolecular potential. The LJ potential has been applied for liquid argon successfully, and is also used as a generic potential not involving specific substances. The LJ interaction is characterized by its strongly repulsive core (the short-distance behavior) and weakly attractive tail. To maintain the reasonable accuracy the cutoff distance is sometimes set as 2.5σ, at which the interaction energy is just 0.016 of the well depth.

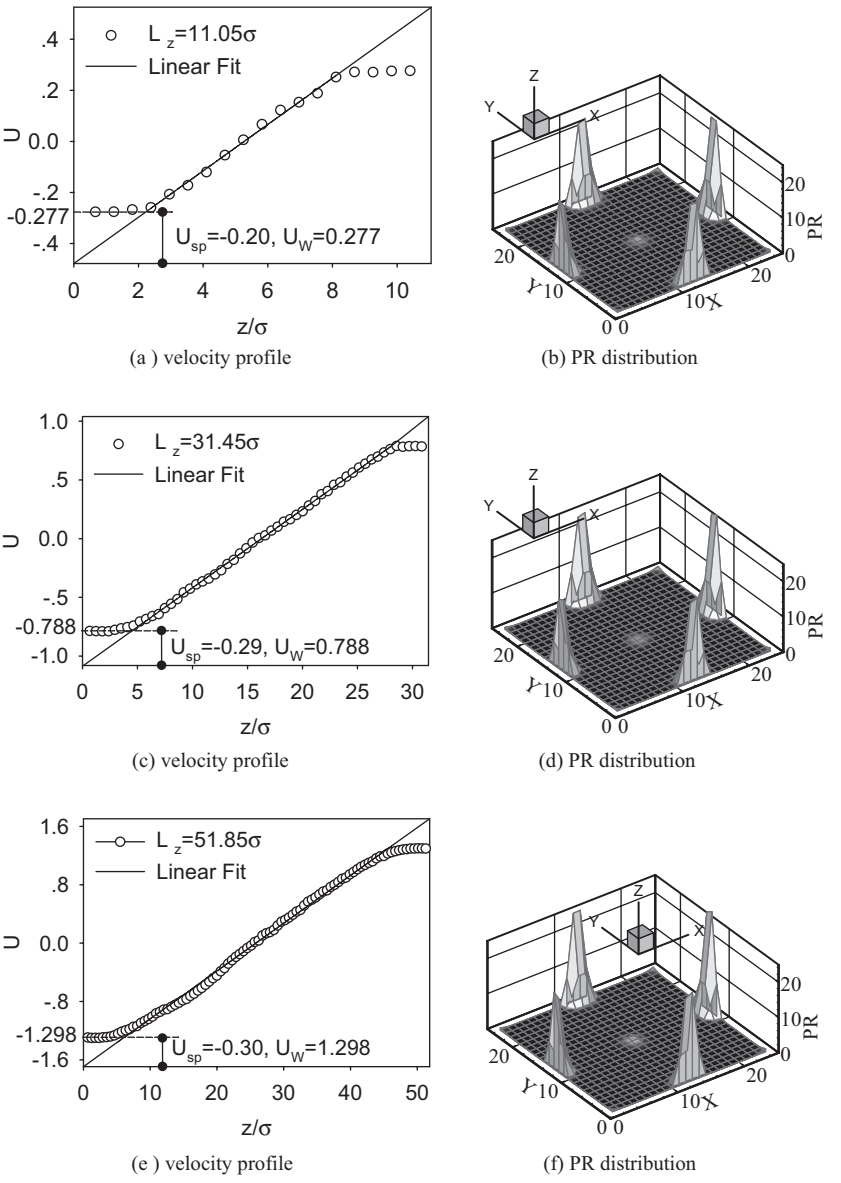

Figure 20. Velocity profile and Pr distributions for three channel heights, $C_1 = 1.0$, $C_2 = 4.0$, $C_3 = 0.76$, $\gamma = 0.05$.

A slight change to the LJ interaction leads to a potential that is entirely repulsive and very short ranged. The particles represented by this potential are little more than soft spheres. Another version of the LJ potential maintains just the r^{-12} term. Any system subject to the LJ potential can exist in the solid, liquid, or gaseous state. The attractive part of the potential is to bind the system for the solid and liquid states, and the repulsive part is to prevent collapse. Other functional forms can be used for interactions between atoms, and between small molecules in cases where spherical symmetrical applies. Some of them

are proven to be more suitable than others for specific problems. An alternative of the LJ potential for use in simple cases is a function in which the r^{-12} term is replaced by $A\exp(-\alpha\gamma)$ [13].

Even though the present three-atom model is developed based on the fcc structure of the solid atoms, the theory can be extended to other microstructures, providing that the solid atoms are arranged orderly and display the periodic array. The simple development of the three-atom model shows that the strong good-potential behavior should be satisfied, with the short distance interactions between molecules. The LJ potential among the three atoms is a perfect good-potential. The three-atom model is valid for the quasi-LJ potentials, but the critical value of the criterion number may be deviated from 0.757. Future work is suggested for other microstructures and intermolecular potentials.

CONCLUSIONS

In this article, a simple but effective three-atom model is developed. The model is limited by the fcc structure of the solid atoms and the well-known LJ potential for the liquid argon. However, it can be possibly extended to other micro systems, providing the solid atoms are arranged orderly and display the periodic nature and the quasi-LJ potential. An important criterion number is developed by the three-atom model, governing the boundary conditions in nanoscale. The theory is consistent with the molecular dynamics simulation. When the criterion number is approaching the critical value of 0.757, the degree of slip is decreased or the degree of locking is increased. Deviation from the critical value results in the increased degree of slip. At the fixed criterion number, higher energy scale ratio between solids and liquids yields the increased degree of locking or the decreased degree of slip. The strong locking boundary conditions have the extended fcc structure for several liquid layers nearest the solid walls. The two micro systems have the same boundary conditions if they have the same criterion number. The slip length is well correlated in terms of the theory.

REFERENCES

1. P.A. Thompson, M.O. Robbins, Shear Flow Near Solids: Epitaxial Order and Flow Boundary Conditions, *Physical Review A*, vol. 41, (12), pp. 6830–6837, 1990.
2. P.A. Thompson, S.M. Troian, A General Boundary Condition for Liquid Flow at Solid Surfaces, *Nature*, vol. 389, pp. 360–362, 1997.
3. J. Koplik, J.R. Banavar, J.E. Willemsen, Molecular Dynamics of Poiseuille Flow and Moving Contact Lines, *Physical Review Letters*, vol. 60, pp. 1282–1285, 1989.
4. P.A. Thompson, M.O. Robbins, Simulations of Contact Line Motion: Slip and the Dynamic Contact Angle, *Physical Review Letters*, vol. 63, pp. 766–769, 1989.
5. J. Koplik, J.R. Banavar, Corner Flow in the Sliding Plate Problem, *Phys. Fluids*, vol. 7, pp. 3118–3125, 1995.
6. S. Richardson, On the No-Slip Boundary Condition, *Journal of Fluid Mechanics*, vol. 59, pp. 707–719, 1973.
7. L.M. Denn, Issues in Viscoelastic Fluid Mechanics, *Annual Review of Fluid Mechanics*, vol. 22, pp. 13–34, 1990.
8. M. Gad-el-Hak, The Fluid Mechanics of Microdevices—The Freeman Scholar Lecture, *Journal of Fluids Engineering*, vol. 121(5), pp. 5–33, 1999.

9. A.A. Rostami, A.S. Mujumdar, N. Saniei, Flow and Heat Transfer for Gas Flowing in Microchannels, A Review, *Heat and Mass Transfer*, vol. 38, pp. 359–367, 2002.
10. S.Y. Liem, D. Brown, J.H.R. Clarke, Investigation of the Homogeneous-Shear Non-Equilibrium Molecular Dynamics Method, *Physics Review A*, vol. 45(6), pp. 3706–3713, 1992.
11. J.L. Xu, Z.Q. Zhou, X.D. Xu, Molecular Dynamics Simulation of Micro-Poiseuille Flow for Liquid Argon in Nanoscale, *International Journal of Numerical Methods for Heat and Fluid Flow*, vol. 14(5), pp. 664–688, 2004.
12. C.L. Tien, A. Majumdar, F.M. Gerner, *Microscale Energy Transport*, Taylor & Francis, Washington D.C., 1997.
13. D.C. Rapaport, *The Art of Molecular Dynamics Simulation*, Cambridge University Press, Cambridge, 1995.